Nonlinear elasticity of an α-helical polypeptide: Monte Carlo studies

Buddhapriya Chakrabarti[1,2] and Alex J. Levine[1,3]
[1]*Department of Physics, University of Massachusetts, Amherst, Massachusetts 01003 USA*
[2]*Department of Physics, Harvard University, Cambridge, Massachusetts 02138, USA*
[3]*Department of Chemistry & Biochemistry and California Nanosystems Institute, University of California, Los Angeles, California 90095, USA*
(Received 17 November 2004; revised manuscript received 12 June 2006; published 6 September 2006)

We report on Monte Carlo studies of the elastic properties of the helix-coil wormlike chain model of α-helical polypeptides. In this model the secondary structure enters as a scalar (Ising-like) variable that controls the local chain bending modulus. We characterize the nonlinear elastic properties of these molecules including their response to applied tensile forces and bending torques both individually and in combination. We find a pronounced effect of applied torque on the extensional compliance of the molecule and a similar effect of tension on the bending compliance. Finally we speculate that the strongly nonlinear response of α-helical polypeptides to combinations of torque and force plays a role in allosteric transitions in proteins.

DOI: 10.1103/PhysRevE.74.031903 PACS number(s): 87.14.Ee, 87.10.+e, 82.35.Lr

I. INTRODUCTION

The mechanical properties of semiflexible biopolymers such as F-actin are generally described by the wormlike chain Hamiltonian [1,2], which treats the filament as a one-dimensional elastic continuum without internal structure. Experiments based on single-molecule manipulations [3–10] have demonstrated the essential validity of this coarse-grained approach to the investigation of biopolymer statistics and mechanical properties. Understanding both the scattering function of such semiflexible polymers in dilute solution [11] and the force extension relations [12] of single semiflexible polymers are among the principal successes of this coarse-grained description of these polymers. A simplification of this nature, although valid in numerous contexts, must break down under forces that are large enough to modify the local structure of the polymer. For example the wormlike chain Hamiltonian ignores the double-helical structure of DNA and the local secondary structure of polypeptides. This local molecular structure controls the bending modulus of the polymer and can be disrupted under applied stress.

This limitation of the wormlike chain (WLC) model is becoming increasingly apparent as researchers probe the mechanical properties of biopolymers under larger applied forces where such a coupling between local molecular structure and chain elasticity plays an important role [13,14]. Such large forces are not only experimentally accessible but are also biologically relevant in such processes as those associated with DNA looping [15,16] and in protein conformational change. An example of the latter process can be found in the conformational change of the protein calmodulin that involves the buckling of a single, solvent-exposed α-helical domain upon the binding of Ca^{2+} ions [17–20]. A polymer model of the α-helical domain that incorporates this nonlinear elastic response of the chain is therefore required to explore conformation change. We expect that such a model as presented here will be directly relevant to the equilibrium mechanics of α-helical polypeptides and more broadly applicable to stiff biopolymers having internal structure, such as DNA.

Recently we [21,22] and others [16,23] proposed a minimal extension of the wormlike chain called the helix-coil wormlike chain (HCWLC) to describe the mechanics of biopolymers with internal structure. This model couples the conformational degrees of freedom of the polymer backbone to localized structural transitions of the constituent monomers by postulating that the local bending modulus of the wormlike chain depends on the local degree of internal structure (the helix or coil variable). For example, the bending modulus of an α-helical polypeptide depends on the local presence of secondary structure and the consequent hydrogen bonding that substantially stiffens the chain. The fundamental result of this coupling is to make both the torque and force response of the polymer highly nonlinear due to localized denaturation events (loss of local secondary structure) under applied force or torque. These denatured regions introduce more compliant elements into the chain, leading to abrupt changes in the effective moduli of the polymer at a critical applied stress.

In this paper we examine, via Monte Carlo simulations, the nonlinear response of the HCWLC to force, to torque, and to the simultaneous application of both force and torque. This simple model of biopolymers with internal structure incorporates a nonlinear coupling between the response of the molecule to applied torques and to tensile forces. This nonlinear coupling is mediated by the secondary structure variables. Thus the nontrivial response of the polymer to combinations of force and torque is made possible by the presence of an ordered (i.e., native) state of the chain. Below we suggest that this nonlinear interaction between bending torques and chain extension may play a role in the allosteric changes frequently observed in natural proteins.

Finally the numerical work reported here complements our previous analytic calculations of the extension and bending compliances of α-helical polypeptides. We can now study features of the HCWLC model that are essentially inaccessible in previous analytic treatments [22] that were based on mean-field descriptions of the secondary structure variables. Thus, we are better able to determine the mechanical properties of weak helix formers, which admit large secondary structure fluctuations in equilibrium. We provide and

test a Ginzburg criterion [24] to discuss the limits of validity of the previously used mean-field approximation.

To briefly review the phenomenology of the model, we reported a mechanical instability of the chain under bending akin to a "buckling instability" in which a segment of an α-helical polypeptide locally melts to form a denatured (random coil) segment beyond a critical angle. At this point the torque required to hold the chain at larger angles drops precipitously. Upon application of a tensile force to the α-helical polymer we find four regimes of response. Arbitrarily small forces break the rotational isotropy of the molecular configurations by orienting the long axis of the molecule in the direction of the applied force. At the low forces, the tension pulls out the small equilibrium undulations of the stiff α-helical polymer in a manner identical to that of the WLC. In the WLC model the extensional compliance of the chain vanishes in the limit of large forces because each segment of the chain is inextensible. This is not the case for the HCWLC. For short enough chains (quantified below) the standard Marko-Siggia [12] plateau in which additional force does not produce extension is replaced by what we term a "pseudoplateau" characterized by the fluctuations of the polymer into the random-coil or denatured state. Since the random-coil sections of the chain are longer than the same segments in their native, α-helical state, the biasing of the fluctuations into the random coil leads to additional contour length of the polymer. Finally in the fourth regime the chain is completely denatured by the applied force and reaches a true Marko-Siggia plateau upon further increasing the force.

The remainder of the paper is organized as follows. In Sec. II we introduce the α helix Hamiltonian based on a combination of the wormlike chain and the helix-coil model. We also discuss the details of the Monte Carlo simulation. The simulation results are analyzed in the Sec. III. We first study the equilibrium properties of the polymer under no applied forces or torques in Sec. III A. We then turn to the bulk of our studies in examining the mechanical properties of the chain under (i) applied torques and no tensile forces in Sec. III B 1, (ii) applied forces but no torques in Sec. III B 2, and (iii) the combination of both torques and forces in Sec. III B 3. We summarize and discuss our results in Sec. IV.

II. THE HELIX-COIL WORMLIKE CHAIN MODEL

The wormlike chain [1,2] is the simplest coarse-grained model for semiflexible polymers. It describes the single-chain polymer statistics in terms of a Hamiltonian that associates an energy cost with chain curvature by introducing a bending modulus κ. In terms of a discretized chain model described by the set of monomeric tangent vectors $\hat{t}_i$, $i=0,\ldots,N-1$ with N the degree of polymerization, the WLC Hamiltonian may be written as

$$H_{\mathrm{WLC}} = \kappa \sum_{i=0}^{N-1} [1 - (\hat{t}_i \cdot \hat{t}_{i+1})]. \tag{1}$$

The bending modulus κ determines the thermal persistence length of the chain, i.e., the distance along the chain over which the tangent vectors decorrelate.

The response of a single chain to extensional forces has been used to understand the deformational properties of biopolymers and their aggregates [12,25,26]. To account for the internal degrees of freedom along the chain a new set of variables is needed. Workers have previously employed the helix-coil (HC) model [27] in order to introduce such internal state variables along the arc length of the chain. This model has been used to study a class of protein conformational transitions [28,29] in solution and under tension [30].

The HC model Hamiltonian, which is used to study these structural transitions, can be reduced to its simplest form by assuming that the local structure of the chain is described by a set of two-state variables $s_i = \pm 1$, $i=0,\ldots,N$. For the α-helical chains of current interest we regard these two states as the conformation of the segment in its native, α-helical state ($s=+1$) and in a disordered, random coil state ($s=-1$).

The elementary units of the chain as described by the HCWLC model are not the amino acid monomers but rather turns of the α helix since it is necessary to unambiguously ascribe the presence or absence of secondary structure to each elementary unit of the model. In practice we expect this level of coarse graining to mean that each segment of the chain (or elementary unit) is composed of ~three monomers.

The coupling of the secondary structure variables to the WLC tangent vectors is effected by introducing a bending stiffness in the WLC Hamiltonian that depends on the local degree of secondary structure. We choose

$$\kappa(s) = \begin{cases} \kappa_> & \text{if } s = +1, \\ \kappa_< & \text{if } s = -1. \end{cases} \tag{2}$$

Due to the hydrogen bonding between turns of the α helix, it is reasonable to expect that $\kappa_>$, the bending modulus in the native state, is significantly larger than $\kappa_<$, the bending modulus of the chain in the non-native, disordered state. Simple estimates of this difference in bending moduli were computed in [22]. Based on those estimates it is possible that $\kappa_>$ is as much as two orders of magnitude larger than $\kappa_<$ for α-helical polypeptides.

The Hamiltonian of the helix-coil wormlike chain may then be written as

$$H = \epsilon_{\mathrm{w}}/2 \sum_{i=0}^{N-1} (1 - s_i s_{i+1}) - h/2 \sum_{i=0}^{N} (s_i - 1) + \sum_{i=0}^{N-1} \kappa(s_i)[1 - (\hat{t}_i \cdot \hat{t}_{i+1})], \tag{3}$$

where ϵ_{w} is the free energy cost of a domain wall in the secondary structure sequence. It is the natural logarithm of the chain cooperativity parameter. h represents the free energy cost per monomer to be in the non-native (i.e., random-coil) state, while $\kappa_>$ and $\kappa_<$ are the bending moduli of the chain in the helix and coil phases as mentioned above. A pictorial representation of the system is shown in Fig. 1.

The full Hamiltonian given by Eq. (3) has four constants with dimensions of energy, $\kappa_>, \kappa_<, h, \epsilon_{\mathrm{w}}$ that can be fitted from experiment. We measure all these energies in units of $k_{\mathrm{B}}T$. We have disregarded the twist degree of freedom of the molecule. Such twist degrees of freedom and the coupling of

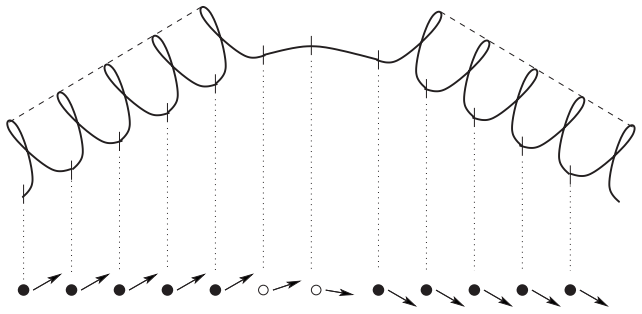

FIG. 1. Schematic figure of an α-helical polypeptide and its representation in the HCWLC. The upper figure shows an α-helical polypeptide with one denatured segment. The dashed line represents intramolecular hydrogen bonding. The lower figure shows the representation of this molecular configuration in terms of the Ising-like secondary structure variables (open circles for random coil segments and filled ones for α-helical ones) and the tangent vectors to the segments of the chain (denoted by arrows). Each basic unit of the model (monomer) is shown between dotted lines.

twisting and stretching modes of these chiral molecules have been explored particularly with regard to the mechanical properties of DNA [31,32]. Also in the present work we evaluate the model in two dimensions. Full three-dimensional variants of the calculation that incorporate torsional modes as well as the twist-stretch coupling are currently under investigation [33]. We also ignore nonlocal steric interactions between segments of the chain. We expect these to not play a significant role in the predominantly ordered states of the molecule due to its long thermal persistence length.

We performed Monte Carlo simulations of the HCWLC in two dimensions using a standard Metropolis algorithm. The system consists of a one-dimensional set of N lattice sites having two variables: an Ising variable $s_i = \pm 1$ specifying the presence or absence of secondary structure, and a continuous angular variable θ_i describing the angle of the local chain tangent vector $\hat{t}_i$ with respect to the x axis. The number of tangent vectors in the simulation is one less than the total number of spins. The energy of a particular HCWLC configuration is given by the Hamiltonian Eq. (3).

We performed two classes of Monte Carlo moves: (i) attempts to change the local secondary structure $s_i \rightarrow -s_i$, and (ii) tangent vector moves $\theta_i \rightarrow \theta_i \pm \Delta\theta$ allowing the chain to explore all conformations. We found that choosing $\Delta\theta = 0.01$ allowed us to equilibrate the chain reasonably rapidly while being small enough so that the discretization of the chain conformations did not significantly affect the numerical results. This latter point was checked by a comparison to runs with even smaller values of the angular variable updates. We studied systems of sizes ranging from $N=10$ to 100 and saw only a small system-size dependence in the sharpness of the transitions of the underlying spin variables.

Before taking data, we equilibrated the system by performing a number of Monte Carlo moves that is greater than four times the longest correlation time in the system. Because of their discrete nature the spin variables equilibrate much faster than the angular variables. Due to the wide separation of the time scales for the equilibration of the helix-coil and angular variables, a more efficient Monte Carlo scheme could be developed by updating the angular variables more often than the secondary structure variables when deep in the ordered phase of these secondary structure variables. We did not pursue such improvements of the efficiency of the code.

We benchmarked our code by comparing our results to the known equilibrium properties of the Ising model and the Kratky-Porod model in the limit where we had artificially frozen either the tangent vectors or the spin variables, respectively. In these cases the HCWLC model reduces to these well-studied cases.

III. RESULTS

A. Equilibrium properties: The radius of gyration

We first investigate an equilibrium property of the unstressed chain using the full HCWLC model by examining its radius of gyration [11,34]. We note that the projection of the polymer arc length along the average tangent vector of a segment, i.e., the effective length of the segment depends on the state of secondary structure. To account for this aspect of the coarse-grained HCWLC polymer model we define a segment length that is a function of the secondary structure variable s_n via

$$\gamma(s) = \begin{cases} \gamma_< & \text{if } s = +1, \\ \gamma_> & \text{if } s = -1, \end{cases} \tag{4}$$

where, as the notation suggests, $\gamma_< < \gamma_>$. The length of a segment increases when it loses its α-helical secondary structure. Based on typical α-helical structures we estimate that $\gamma_> = 3\gamma_<$. Unless explicitly stated otherwise, we fix the ratio of segment lengths to this value. Furthermore, we take the total contour length L of the chain with polymerization index N to be $N\gamma_>$, the length of the fully straightened and denatured molecule.

The separation vector between the ith and jth segments along the chain is given by

$$\vec{R}_{ij} = \sum_{n=i}^{j-1} \gamma(s_n)\hat{t}_n, \tag{5}$$

where $\gamma(s_n)$ is the length of the nth segment measured along its mean chain tangent as defined above.

To compute the radius of gyration in our simulations we first evaluate the center of mass of the polypeptide, which is given by

$$\vec{R}_{\text{c.m.}} = \frac{1}{N}\sum_{j=1}^{N}\sum_{i=1}^{j} \gamma(s_i)\hat{t}_i. \tag{6}$$

The radius of gyration is then evaluated by computing the average

$$R_G^2 = \frac{1}{N}\left\langle \sum_{j=1}^{N}\left(\sum_{i=1}^{j} \gamma(s_i)\hat{t}_i - \vec{R}_{\text{c.m.}} \right)^2 \right\rangle. \tag{7}$$

We plot in Fig. 2 the radius of gyration as a function of h for $\epsilon_w = 10$, and bending moduli $\kappa_> = 100$ and $\kappa_< = 1$ for an (N

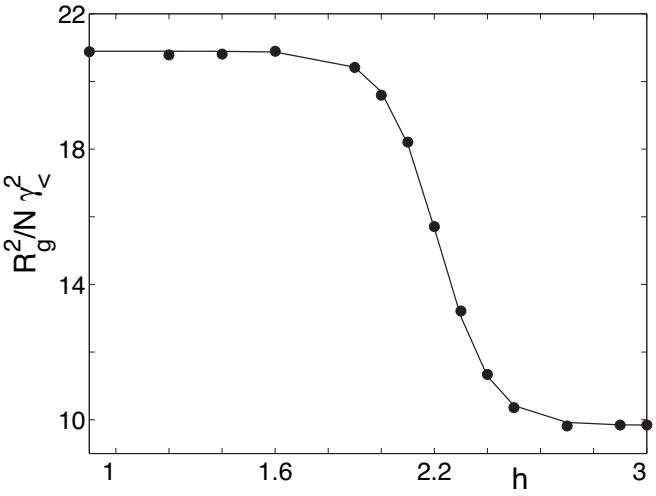

FIG. 2. Radius of gyration of the HCWLC as a function of the free energy cost per segment to transform to the random coil, non-native state: h obtained from Monte Carlo simulations (plotted using black dots) as compared with the theory [22]. In this curve $\kappa_>=100$, $\kappa_<=1$, $N=10$, and $\epsilon_w=10$. All the energy scales are measured in k_BT and the error bars are smaller than the symbols in the plot.

=10)-sized chain obtained using Monte Carlo simulations (black dots). These data are in excellent agreement with our analytic calculations (solid line) [22]. The energy scale h is the free energy cost of a polymer segment being in its non-native (i.e., random-coil) state. Variations of h mimic the modification of the solvent quality as is done in the denaturation of proteins by the addition of, e.g., guanidinium [35]. Figure 2 reflects the decrease in the radius of gyration with an increasing thermodynamic driving force toward the native (α-helical) state of the molecule. This decrease is the result of two competing effects: (i) each chain segment shrinks in length upon adopting its native state ($\gamma_> \to \gamma_<$), shortening the radius of gyration, and (ii) the longer persistence length in the native state ($\kappa_< \to \kappa_>$) increases the overall radius of gyration. For physiologically reasonable parameter values we find that the former effect dominates so that the net result is a decrease in R_G as the polymer adopts its native state structure.

Another effect of solvent quality is the change in the effective excluded volume interaction between segments of the polymer. This effect is not included here. We expect that for small values of the polymerization index N this effect of solvent quality plays a subdominant role.

Similar behavior is seen in other measures of the polymer size in solution such as the average squared end-to-end vector of the chain. For high chain cooperativity and h chosen so that the chain is in either the all-helix or all-coil phase, we find this quantity has the expected WLC form: $\Delta R^2 = N^2\gamma^2 g(N\gamma/l_p)$, where $g(x)=2[\exp(-x)-1+x]/x^2$ and γ is either $\gamma_<$ or $\gamma_>$ for the all-helix or all-coil chains, respectively. At intermediate values of h, the behavior of the HCWLC is similar to the WLC but with a persistence length and segment size that interpolate between those of the helix and the random coil. This result also agrees with previous analytic calculations [22].

B. Mechanical compliances

1. Bending compliance

We begin our exploration of the mechanical properties of the model by considering the response of the chain to externally applied torques in thermal equilibrium. These torques act to constrain the tangent vectors of the ends of the molecule while not applying tensile stress. There are two conjugate thermal ensembles that can be studied to consider the bending compliance. The first is a fixed bend ensemble in which the angular deviation of the first and last chain tangents is fixed, and the second is an ensemble in which the tangent vectors of all chain segments are unconstrained and a fixed torque is applied to the chain via force couples applied to the first and the final chain segments. In the former ensemble one can compute in closed form the thermally averaged torque required to enforce the constraint on the chain tangents. Here we expect the results of the simulations to agree with these previous calculations. The response of the system to a fixed torque, which is likely of more direct experimental interest, cannot be as simply determined. Moreover, the response of the chain to a combination of tensile stress and bending torques cannot be computed analytically in closed form. We address the more general problem of the response of the polymer to a combination of applied forces and torques in Sec. III B 3.

We consider first the fixed chain tangent ensemble. We hold the first tangent vector fixed along the $\hat{x}$ axis and constrain the last chain tangent to make a fixed angle ψ with respect to the same axis. We numerically evaluate the constraining torque $\tau(\psi)$ by computing the derivative of the free energy with respect to the angle ψ. In our simulations this is effected by directly calculating the thermal average

$$\tau(\psi) = \langle \kappa(s_{N-1})\sin(\psi - \theta_{N-1})\rangle. \tag{8}$$

The results, which corroborate the analytic calculations, are plotted in Fig. 3. At small values of the bending angle ψ, there is a linear dependence of the constraining torque on ψ. The α helix bends like a flexible elastic rod. At a certain critical angle $\psi^\star$, however, the constraining torque reaches a maximum and then drops precipitously for angles $\psi > \psi^\star$ as shown in Fig. 3. This dramatic collapse of the chain's rigidity is akin to the buckling instability of a macroscopic tube such as a drinking straw. The mode of the localized failure though is quite different. Here the failure is caused by the localized disruption of the secondary structure. The breaking of the hydrogen bonds at this denatured site introduces a weak link allowing the molecule to bend at a lower torque. At $\psi=\psi^\star$, M, the fraction of the chain in the non-native state, abruptly jumps to $O(1/N)$, demonstrating that, within the model, the buckling failure is due to the creation of a single random-coil segment along the chain that provides a region of greatly reduced bending stiffness. The size of the created random-coil section will remain on the order of $N\kappa_{\langle/\kappa\rangle}$ so for a large difference in bending moduli between the native and non-native states of the chain, these "weak links" generically occupy a small fraction of the polymer. For instance, in the example shown in Fig. 3 there is only one weak link created.

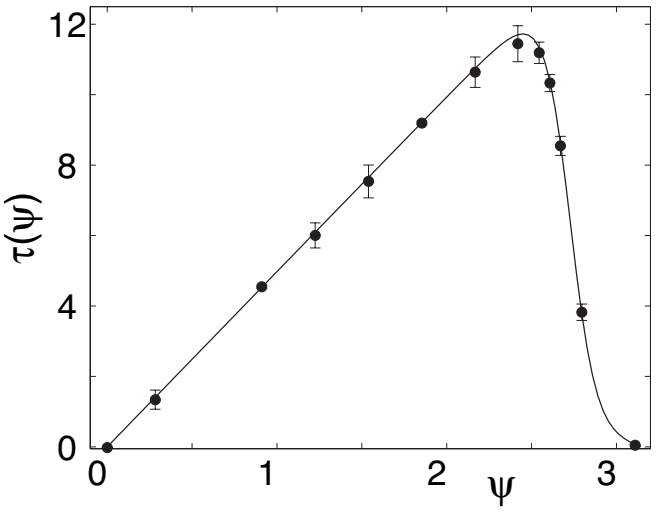

FIG. 3. Numerical torque vs angle data (filled points) for $\epsilon_w = 8.0$, $h = 10.0$, $\kappa_> = 100$, and $\kappa_< = 1$ compared with previous exact calculations [13,14] (solid line) for an $N = 10$ chain. The torque is measured in units of k_BT. The error bars are not shown where they would be smaller than the size of the points.

The above behavior is seen in the parameter range (ϵ_w, h) consistent with the chain being in an all-helix state in thermal equilibrium in the absence of applied torque. If the equilibrium system is in a mixed helix-coil phase such behavior is not observed. Instead we see a monotonic increase in the bending torque for all end angles less than π as expected for an elastic rod. At $\psi = \pi$ the torque measured in thermal equilibrium is identically zero since one is averaging a signed quantity (the projection of the torque vector out of the plane) and the statistical weight of positive and negative torques becomes equal. The average of the squared torque, however, vanishes only at $\psi = 0$ modulo 2π. Since it is reasonable to suppose that the chain bends in the plane defined by first and last constrained chain tangents, one expects that our two-dimensional results accurately capture the buckling instability of the chain. We expect that the full three-dimensional calculation would generate at least qualitatively similar results.

2. Extensional compliance

We now study the extensional compliance of α-helical polypeptides, which is the most easily accessible mechanical property of the chain by current experiments. We consider the thermally averaged extension of the chain in the direction of an applied force acting on one end of the tethered molecule. Based on previous mean-field calculations [22] we expect there to be four force regimes where the extensional compliance of the molecule is due to differing modes of extension. At the lowest forces the principal effect of the applied force is to orient the long axis of the molecule that is typically much shorter than its own thermal persistence length in the stiffer α-helical phase. At still higher forces, the applied tension will begin to decrease the thermal population of transverse undulations along the α helix and thereby increase its mean length. This is the source of the extensional compliance of the WLC. At still higher applied tensions where these transverse undulations are severely depleted, we expect additional tensile force to induce chain segments to fluctuate into their more extended, random coil phase. This small additional extension due to rare fluctuations into the random coil provides a small additional compliance, leading to a regime of slowly increasing chain length with increasing tension—the "pseudoplateau" in the extension vs force curve. Finally, at still higher forces we expect to denature the chain and thereby liberate more stored length over a narrow range of tension leading to a longer WLC with a lower effective persistence length. We now study the range of validity of these mean-field predictions and examine the extensional compliance of the chain in a parameter regime where this mean-field analysis fails.

In the presence of a tensile force F, the Hamiltonian of the HCWLC may be written as

$$H = H_0 - F\sum_{i=0}^{N} \gamma(s_i)\cos(\theta_i), \tag{9}$$

where H_0 is the HCWLC Hamiltonian in the absence of externally applied forces as shown in Eq. (3). In our Monte Carlo simulations we apply a force of magnitude F and then equilibrate the chain as described above. We calculate the mean length of the chain as a function of the externally applied force using

$$L(F) = \left\langle \sum_{i=1}^{N} \gamma(s_i)\hat{t}_i \cdot \hat{x} \right\rangle. \tag{10}$$

In Fig. 4 we observe in the lower panel three of the four extension regimes predicted by the mean-field calculation beginning with the pulling out of transverse undulations in the stiff α helix at small applied tensions $F < F_-$. The lower force F_- is determined by the beginning of the first Marko-Siggia plateau where the amplitude of transverse thermal undulations of the all-α-helical polymer have been significantly reduced. Because that reduction has an algebraic dependence on applied force, it is not possible to unambiguously select a critical force marking the onset of the plateau. It appears reasonable, however, to insist that the plateau has been reached when $(dL/dF)(1/\gamma_<^2) \ll 1$, i.e., when the incremental extension of the chain measured in monomer lengths $\delta L/\gamma_<$ is small for a change in force $\delta F \sim 1/\gamma_<$ set by the thermal energy $(k_BT = 1)$ divided by the same monomer size. In this case we find the force associated with the plateau onset

$$F_- \sim N^{2/3}\kappa_>^{-1/3}\gamma_<^{-1} \tag{11}$$

grows with the length of the chain. Longer chains require larger forces to sufficiently pull out the equilibrium population of transverse undulations and thereby reach the plateau regime.

At larger tensions $F > F_-$ we enter the pseudoplateau (in the lower panel of Fig. 4) where the molecule in the all-helical phase has already asymptotically approached its maximum length $N\gamma_<$ as $1/\sqrt{F\kappa_>\gamma_</k_BT}$. The WLC predicts the vanishing of the extensional compliance as the chain reaches its maximum length; this would produce a true pla-

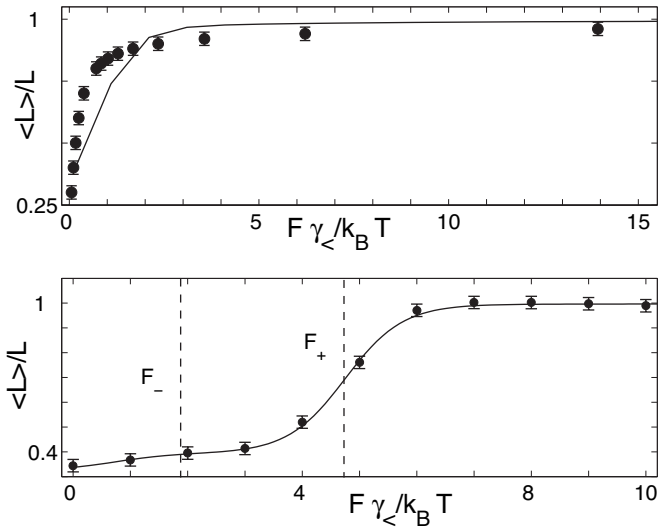

FIG. 4. Force vs extension Monte Carlo data (points) and mean-field theory (solid line). For the upper panel the parameters are $\epsilon_w=0.5$, $h=1.0$, $\kappa_>=4.0$, $\kappa_<=2.0$, and $N=20$. In the lower panel the parameters are $\epsilon_w=8$, and $h=1.5$, and $\kappa_>=100$, $\kappa_<=1$, and $N=10$. In each the mean length of the chain normalized by the maximum chain length $N\gamma_>$ is plotted as a function of the applied force normalized by the length of a helix segment $\gamma_<$. A comparison of the two figures demonstrates the disappearance of the pseudoplateau (intermediate-force flat region) for sufficiently long or uncooperative chains.

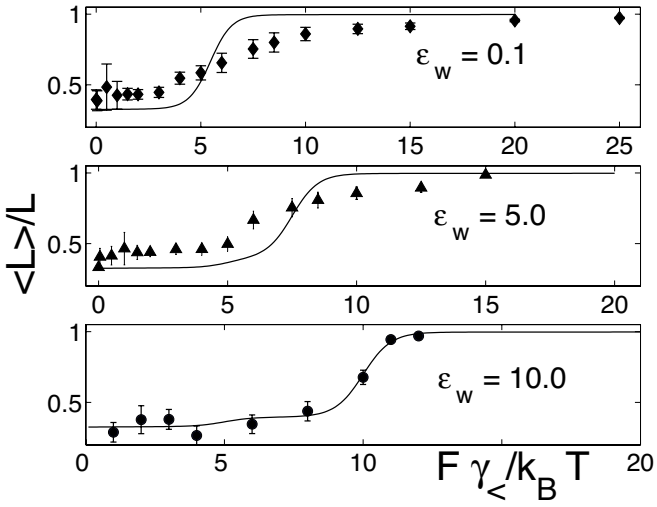

FIG. 5. Force vs extension Monte Carlo data (points) shown in the low (top panel), intermediate (middle panel), and high (bottom panel) cooperativity limit. In each the mean length of the chain normalized by the maximum chain length $N\gamma_>$ is plotted as a function of the applied force normalized by the length of a helix segment $\gamma_<$. The parameters are $h=10.0$, $\kappa_>=100.0$, $\kappa_<=1.0$, and $N=20$, and $\epsilon_w=0.1$ (top panel), 5.0 (middle panel), and 10.0 (bottom panel). The solid lines correspond to the mean-field calculation [22].

teau at these intermediate forces. This plateau, however, is not flat in the HCWLC due to the fact that an increase in the applied force enhances the fluctuations into the longer, random-coil phase of the segments, which we refer to as the pseudoplateau. The end of this plateau is marked by a sharp lengthening transition at a value of force

$$F_+ \approx \frac{\epsilon_w + h}{\Delta\gamma} \tag{12}$$

where $\Delta\gamma=\gamma_>-\gamma_<$. At tensions larger than F_+ we observe the force-induced denaturation of helical domains. F_+ is determined by balancing the free energy cost associated with transforming a segment from α helix to random coil with the work done by the external force during that transformation: $h+\epsilon_w \sim \Delta\gamma F_+$. The width of the pseudoplateau is controlled by two forces, a force of onset F_- and a maximum force F_+ at which point the abrupt denaturation transition occurs. For the appropriate parameter values these forces are marked by dashed lines in the lower panel of Fig. 4.

Upon closer examination of Eqs. (11) and (12) one notes that the existence of the intermediate-force pseudoplateau is actually a finite-size effect; for a large enough polymerization index N the pseudoplateau may vanish as F_- becomes greater than F_+. The tension required to straighten the α helix is large enough to denature the molecule. Since the existence of the pseudoplateau requires that $F_-<F_+$, it will be found only in chains where

$$N \leqslant \left(\frac{h+\epsilon_w}{\gamma_<\Delta\gamma}\right)^{3/2}\kappa_>^2. \tag{13}$$

In the upper panel of Fig. 4 the above inequality is violated so the pseudoplateau vanishes. For still less cooperative chains (smaller ϵ_w) we find the chain in a mixed helix and coil state and we obtain force extension curves similar to those of the WLC results of Marko and Siggia [12].

Typical α-helical polypeptides are quite short $N\sim O(10)$ and stiff $\kappa_>\sim O(10^2)$ so that one expects to observe this pseudoplateau behavior quite generally. We see that, for the parameters used to create the upper panel of Fig. 4, the criterion for the presence of the pseudoplateau is not met and in our Monte Carlo simulations we indeed observe no pseudoplateau for these values. When the criterion is met, as in the case shown in the lower panel of Fig. 4, the mean-field example, the pseudoplateau is evident.

In both panels of Fig. 4, however, the mean-field calculation (solid line) qualitatively agrees with the numerical data (points). That agreement is better for the more cooperative system in the lower panel where $\epsilon_w=8.0$ than in the system shown in the upper panel where $\epsilon_w=0.1$.

Examining Fig. 5 we see the breakdown of the mean-field description of the force extension behavior of the HCWLC. The domain wall energy (and hence the chain cooperativity parameter) increases progressively from the top to bottom panels of the figure. The numerical data are shown as points and the mean-field theory force extension curve for those chain parameter values is shown as the solid line. In the upper panel the denaturation transition significantly deviates from the mean-field theory. The mean-field theory success-

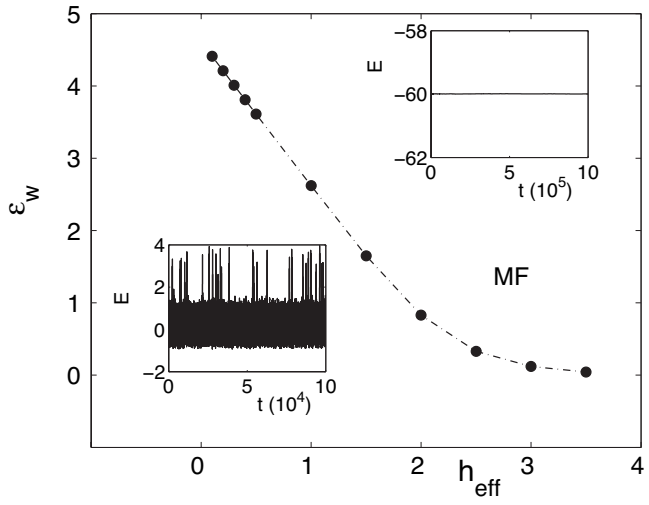

FIG. 6. A map of the ϵ_w-h_{eff} parameter space of the helix-coil degrees of freedom showing the region of validity of the mean-field (MF) approximation as determined by the Ginzburg criterion. The insets show the energy fluctuations over Monte Carlo steps in numerical simulations of the two regimes.

fully predicts the midpoint of the transition, but is unable to account for its width. As ϵ_w is increased in the middle panel the mean-field theory better describes the data although it still fails dramatically in the transition zone at reduced forces of ≈ 6. Finally, at large enough values of the chain cooperativity parameter ($\epsilon_w \approx 8$) the mean-field theory describes the force-extension behavior of the chain with quantitative accuracy.

It is reasonable that the mean-field theory fails to accurately describe the force-extension behavior of the polymer where the chain cooperativity parameter ϵ_w is small since one expects the fluctuations in the polymer's secondary structure to become significant in this limit. These fluctuations are ignored in the mean-field calculation. Measurement of the energy fluctuations of the chain in the Monte Carlo simulation allows one to directly monitor the significance of fluctuations.

Using these measurements of the energy fluctuations we map the region of validity of the mean-field theory in the parameter space spanned by ϵ_w and h_{eff} (defined below) as shown in Fig. 6. To the right of the dashed line (the region labeled MF) the energy fluctuations are small compared to the mean energy and the mean-field theory holds. In the region to the left of this division the system is dominated by large secondary structure fluctuations and large fluctuations in its internal energy. Two traces of the total energy as a function of Monte Carlo time representative of each region are shown as insets. The ratio of the variance of the energy to its mean value is ≈ 2.3 in the fluctuation-dominated regime. In the mean-field regime this ratio is $\approx 10^{-3}$.

To better understand the breakdown of the mean-field theory, we observe that, if the polymer were straight, the effect of the force on the remaining secondary structure variables would be to simply shift the effective free energy cost per segment to destroy the secondary structure from h to $h_{eff}=h-F\Delta\gamma$; the cost of denaturing the segment is h but the net work done by the chain upon extension under the external force F is $-F\Delta\gamma$. We recall that the validity of the mean-field theory requires only the suppression of secondary structure fluctuations. We then expect the mean-field theory to fail where $h_{eff}=h-F\Delta\gamma$ is small, which for reasonable values of h requires significant forces. Assuming that these forces have quenched most of the contour fluctuations of the chain, we take as an approximate criterion for the breakdown of the mean-field theory the Ginzburg criterion for the one-dimensional helix-coil model with an effective field h_{eff}. Thus the mean-field theory is expected to hold when

$$\frac{\langle s_i^2\rangle - \langle s_i\rangle^2}{\langle s_i\rangle^2} \ll 1. \tag{14}$$

Neglecting boundary effects to restore the translational invariance along the chain and taking N large enough so that we may consider only λ_1, the larger of the two eigenvalues of the transfer matrix, this condition can be written as

$$\frac{\lambda_1(\partial^2\lambda_1/\partial h^2)}{(\partial\lambda_1/\partial h)^2} \ll 1 \tag{15}$$

where the larger eigenvalue, computed in [22], is given by

$$\lambda_1 = (1+e^{-h_{eff}}) + \frac{1}{2}\sqrt{(1-e^{-h_{eff}})^2 + 4\exp(-2\epsilon_w - h_{eff})}. \tag{16}$$

This Ginzburg criterion given by the combination of Eqs. (15) and (16) is shown in Fig. 6 as the dashed line. The filled circles represent the numerically determined boundary between the mean-field- and fluctuation-dominated regimes obtained directly from Eq. (14) using our Monte Carlo data. We see that the above analytic expression correctly distinguishes these two regimes.

Figure 6 makes clear that the mean-field theory holds in the limit of high chain cooperativity as expected. We expect that, if the chain parameters are chosen so that the mean-field theory holds at zero force, there will not be significant fluctuation corrections at the denaturation transition due to the low dimensionality of the system.

3. Nonlinear coupling: Bending and extension

We now examine the nonlinear interaction between the responses of the molecule to a combination of applied tensile forces and bending torques. We consider two different ensembles in which we apply a force to the end of the chain while simultaneously (i) constraining the end tangents to differ by an angle of ψ, or (ii) applying a fixed torque to the end tangent of the chain.

To explore the first of these two ensembles we set the angles between the first and last tangents and the x axis to be, respectively, $\theta_1=0$ and $\theta_N=\psi$. We use the numerical code to compute

$$L(F,\psi) = \left\langle \sum_{i=1}^{N} \gamma(s_i)\hat{t}_i\cdot\hat{x} \right\rangle \Bigg|_{\theta_0=0,\theta_N=\psi}, \tag{17}$$

which gives the mean length of the chain.

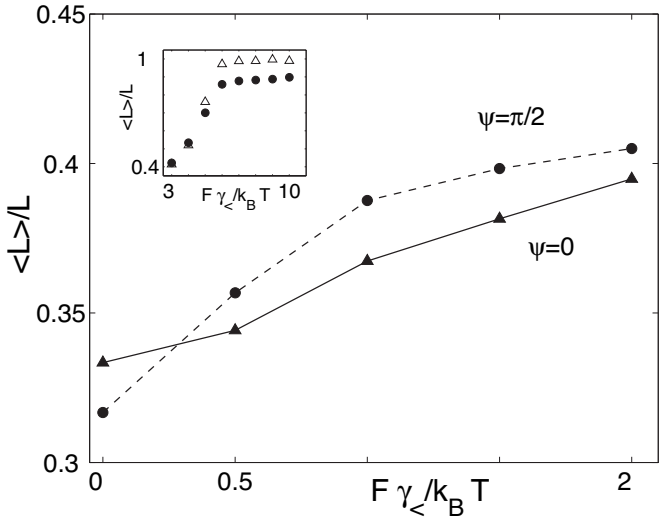

FIG. 7. Force vs extension curves for HCWLC chain with constrained end tangents. The force vs extension is shown for chains where the first tangent lies along the direction of the pulling force while the second tangent makes an angle of $\psi=0$ (triangles) or $\pi/2$ (circles) with respect to the initial chain tangent. The parameters of the chain are $\kappa_>=40$, $\kappa_<=2$, $\epsilon_w=8$, $h=1.5$, and $N=20$. Note that the extensional compliance depends on the state of the final chain tangent. The inset shows that the chain extension in the direction of applied force saturates at high forces to different values as a result of the constrained end tangent.

In Fig. 7 we plot two force extension curves for a HCWLC having parameters $\kappa_>=40$, $\kappa_<=2$, $\epsilon_w=8$, and $h=1.5$. In both cases the initial chain tangent is constrained to lie along the $\hat{x}$ axis, the direction of the tensile force. In one case (triangles) the final chain tangent is collinear with the initial chain tangent so that $\psi=0$, while in the second case (circles) the final chain tangent makes an angle $\psi=\pi/2$ with the initial one.

We note that in the case of the initially bent chain ($\psi=\pi/2$) the tension-free mean length is smaller than that of the straight chain ($\psi=0$). This is simply due to the fact that, in order to minimize bending energy, the thermally averaged trajectory of the bent chain forms the arc of a semicircle and therefore has a smaller projection along the x axis than the $\psi=0$ chain, which is fluctuating about a straight trajectory. The nonzero values of the two chain lengths at zero applied force is a consequence of our fixing the initial tangent vector to lie along the x axis and breaking the rotational symmetry of the problem. Since the native, α-helical state has a thermal persistence length that is longer than the molecule, even at zero force the molecule's projection along the x axis is close to the projected length of the straight and circular segments.

At low applied force we see that the bent chain has a greater extensional compliance than the straight one. The $\psi=\pi/2$ chain reaches its pseudoplateau more rapidly with increasing force. The bending of the chain has shifted the equilibrium constant between denatured and native states of the segments so that under tension there are greater fluctuations into the more extended denatured state in the bent chain than in the straight one. This effect leads to the enhanced extensional compliance of the chain in the bent state for tensile forces that allow the chain to remain predominantly in its native state. Once the chain denatures under further increases in the force, however, the coupling between the extensional compliance and end tangent constraint disappears since the chain now has a severely reduced persistence length. With a persistence length now much shorter than its own arc length, the effect of the constrained end tangent plays a minimal role, affecting only those segments of the chain within one persistence length of the end tangent.

In fact, as one approaches arbitrarily high forces the effect of the constrained end tangent becomes localized at the last segment of chain regardless of the bending moduli of the polymer so that its effect becomes negligible. In the limiting case of infinite force there remains only the effect of the constrained end itself, which decreases the length of the chain by $\gamma_>(1-\cos\psi)$. The high-force regime is shown in the inset of Fig. 7. There we see that for forces large enough to partially denature the chain (beyond the pseudoplateau) the independence of the extensional compliance on ψ, the angle of the end tangent. Additionally we note the asymptotic difference in the lengths of the two chains related to the constraint on the end tangent itself.

Finally, in the strongly fluctuating secondary structure regime, we do not observe any effect on the extensional compliance due to end tangent constraints. These data are not shown. This is to be expected based on the reasoning presented above. Taken together, these results show that in the well-ordered α-helical state, control of the end tangents of the chain can be used to exert control over not only the mean shape of the α helix, but also its mechanical compliances. This control method, made possible by the existence of secondary structure, may be an avenue for the long-range control of protein mechanical properties in one part of the molecule via allosteric changes in another part.

The numerical data presented above do not directly probe the force-torque coupling since we have measured the extensional compliance in an ensemble of chains with fixed end tangents. Clearly, in the constrained end tangent simulations discussed above the constraint torques have a complicated dependence on the extensional stress. In order to quantitatively probe the force-torque coupling it is necessary to work in a fixed torque ensemble rather than a fixed angle one. From the point of view of developing a coarse-grained mechanical description of the an α-helical rod, it is essential to determine the generalized response of the rod to any combination of known forces and torques. To do this we now turn to the statistical measurements of the force extension behavior of the α helix made in the fixed torque ensemble.

In Fig. 8 we plot the extension L of the α helix vs applied tension F for two different values of applied torque on the end tangent of the molecule. The chain parameters are $h=10.0$, $\epsilon_w=8.0$, $\kappa_>=100$, $\kappa_<=1$, and the polymerization index is $N=20$. The values of the torque (in units of k_BT) are taken to be 1 and 10. The former value is taken to be in the range of linear bending response of the polymer in the zero-tensile-force case as can be seen by Fig. 3. The latter value is chosen to be near the maximum torque that the molecule can support without denaturing as shown again in Fig. 3. We note from the figure that at large enough tensions (in this case for $F\gamma_</k_BT>20$) the effect of the applied torque on the exten-

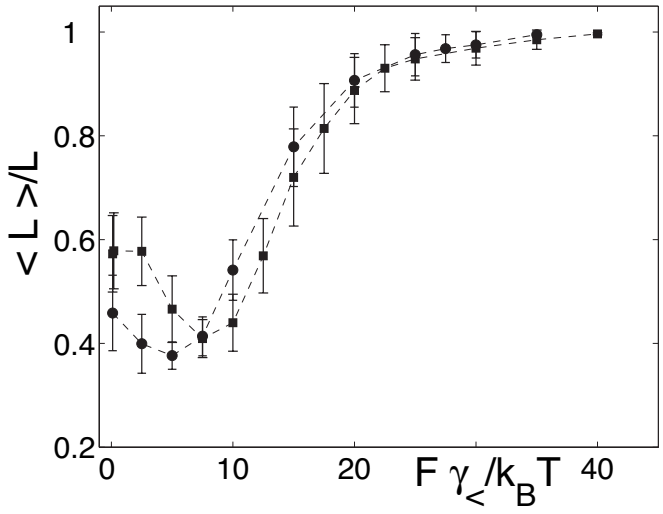

FIG. 8. The extension vs force curves for the HCWLC chain under a fixed torque applied to the last chain segment. The model parameters are given by $h=10.0$, $\epsilon_w=8.0$, $\kappa_>=100.0$, $\kappa_<=1.0$, and the applied torques are $\tau/k_BT=1.0$ (squares) and 10.0 (circles). The dashed lines are guides to the eye.

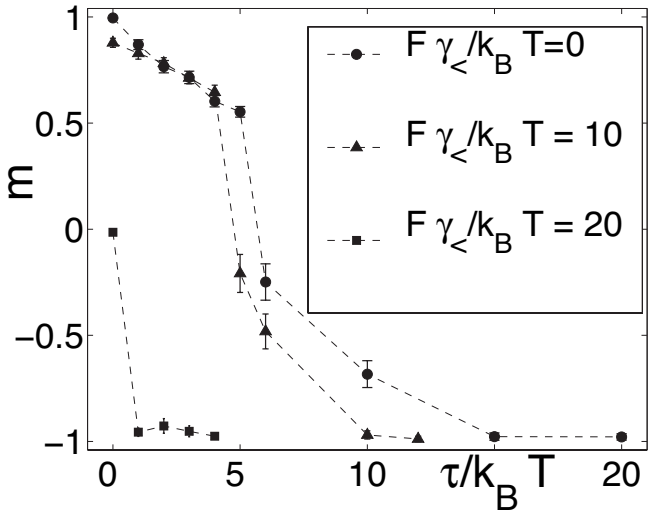

FIG. 9. The torque-induced denaturation of the α helix under applied tension. The secondary structure order parameter m is plotted against the applied torque on the polymer for chains under various tensile stresses. The pretensioning of the chain shifts the free energy difference between the native and denatured states of the molecule thereby weakening its effective bending modulus. The chain parameters are $h=3.0$, $\epsilon_w=8.0$, $\kappa_>=100$, $\kappa_<=1$. The dashed lines are the guides to eye.

sional compliance vanishes. This effect is once again related to the destruction of secondary structure at sufficiently high forces. Without the secondary structure the nonlinear coupling between applied torque and the extensional compliance of the molecule vanishes.

At lower values of the applied force we note the appearance of a local minimum in the extension vs force curve of a depth that increases with applied torque and a position that decreases with increasing applied torque. The region to the left of the local minimum where the extension decreases with increasing force is an unstable region in the force-extension curve that is created by the applied torque. The appearance of this instability in the extension vs force curve is analogous to the region of decreasing equilibrium torque with increasing angle in Fig. 3. In this unstable region increasing force actually leads to a decreasing extension of the polymer.

The underlying cause of this instability can be understood as follows. At no applied tension the fixed torque bends the molecule so that its thermally averaged conformation is that of an arc of a circle. Unlike in the case of the constrained end tangents (data shown in Fig. 7) the particular arc of the circle is not fixed by the constrained tangents but is rather determined by energy minimization, taking into account the applied torque and the effective persistence length of the chain.

At small tensions the applied force has two effects on the chain. First the circular arc, which is the average shape of the molecule, extends along the x axis in response to the force. Second, the applied tension shifts the equilibrium between the native and denatured states of the individual segments toward the more flexible denatured state. Since the molecule is rendered more flexible under the applied tension its mean shape with the same applied torque becomes more bent. This further bending reduces the extension of the molecule along the x axis. The reduced effective thermal persistence length also generates a larger population of transverse thermal undulations along this mean shape. These undulations further reduce the projected arc length of the molecule. The numerical data show that these two shortening effects dominate over the simple stretching of the mean molecular trajectory resulting in a seemingly paradoxical shortening the molecule under applied force.

We can further explore this effect by examining the secondary structure order parameter m, which gives the thermal average of the secondary structure variables of the chain and is defined by Eq. (18):

$$m = \frac{1}{N}\sum_{k=1}^{N} \langle s_k \rangle. \tag{18}$$

The secondary structure order parameter takes values in the range $1 > m > -1$ where a value of +1 represents an all-helix configuration of the molecule while −1 represents a completely denatured chain.

In Fig. 9 we plot this secondary structure order parameter as a function of the applied torque for three different values of applied tension. As is the case in all systems studied in this article, the molecule with no applied forces or torques exists in nearly perfect α-helical state in thermal equilibrium. For smaller applied torques we note that m decreases monotonically. At a critical value of the applied torque τ^*, m begins to drop much more dramatically until it saturates near −1, a completely denatured chain. The value of τ^*, the critical torque, is a strongly decreasing function of the applied tension. At high tensions much less torque is required to

denature the chain than at lower tensions. This rapid decrease in $\tau^{\star}$ with increasing tensile force supports our description of the underlying cause of the instability seen in the extension vs force curves under constant applied torque (Fig. 8).

The appearance of this instability in the force-extension curves under applied torque suggests an interesting application to the understanding of the allosteric properties of proteins. If the α-helical polymer is mechanically coupled to another elastic element under tension in a macromolecule, then the application of torque to the α helix can induce a discontinuous jump in the extension of the helix as this molecular subunit is put into an unstable region of its force extension curve by the applied torque. We expect the α helix to extend past the unstable region in the force-extension curve and equilibrate at a new length at some part on the monotonically increasing region of the extension vs force curve.

IV. CONCLUSIONS

We have numerically explored the nonlinear elastic response of the HCWLC model for α-helical polypeptides to a combination of applied forces and torques. Our Monte Carlo simulations of the extensional compliance of the polymer agree satisfactorily with previous analytic calculations where the mean-field theory is expected to hold as determined by a Ginzburg criterion. The response of the polymer to applied torque at zero tension also agrees with the analytic calculations; this is to be expected as the force-free partition function of the system can be computed exactly.

The typical structure of the extension vs force curve is essentially that of two WLC curves (one for the native state at low tension and one for the denatured state at high tension) that are separated by the pseudoplateau region characterized by small fluctuations of the chain segments into the denatured state. Using the Monte Carlo simulations we have examined regions of parameter space where this typical structure of the curve is changed. For long enough chains (large N) the pseudoplateau vanishes showing that this feature is a finite-size effect. We have also studied the force-extension behavior of the chain in those regions of parameter space where the mean-field model clearly fails. We have found a much smoother crossover from short, stiff helical configurations to longer and more flexible denatured states. This is a reasonable model for weak helix formers. In this fluctuation-dominated regime we find that the equilibrium extension of the chain is well described by a WLC with a persistence length that interpolates between its value in the helix and coil states.

The Monte Carlo calculations provide a nonperturbative approach to investigating the nonlinear coupling between response of the chain to combinations of applied tensile forces and bending torques.

We find that applied torque qualitatively changes the extension vs force curves of the molecule as long as these torques are not so large as to denature a large fraction of the chain. This qualitative change in the extension vs force curves due to applied torque persists to a high force limit where the tensile force finally denatures the molecule. Similarly, constrained end tangents can affect the extensional compliance of the molecule and its mean length. The underlying cause of this nonlinear coupling between the bending and extensional compliances of the molecule is that both applied torque and force shift the equilibrium between the native state and denatured regions of the α helix and thus affect the mechanical properties of the molecule.

One interesting consequence of this coupling is that it is possible to use applied torques or constraints on the end tangents to dramatically modify both the equilibrium length of an α helix under tension and its extensional compliance. In fact applied torque can generate discrete shifts in the equilibrium length under tension; this mechanism for discrete shifts in molecular architecture may help to elucidate the underlying dynamics associated with allosteric transitions in proteins.

Before such detailed modeling of protein conformational change can be attempted, or any other application of this theory to physical systems, a number of physiologically relevant parameter values must be determined. The most difficult of these involve determining the complex intramolecular forces and internal geometry of proteins. The more simple involve fixing the parameter values that describe the single α helix that is the focus of the current work. Determining these basic internal energy scales of an α helix allows one to make quantitative predictions for single-molecule manipulation experiments [38,39] involving simple α-helix formers.

The appropriate energy scales h and ϵ_{w} that describe typical α-helical polypeptides under physiological conditions have been estimated to be $h \approx 1.5$ and $\epsilon_{\mathrm{w}} \approx 7$ for certain chemical systems [36,37]. More generally we expect these energy scales to be of the same order of magnitude for all secondary structure forming polypeptides. For such parameters and polypeptides of no more than $N \sim O(10)$ turns it appears from our Ginzburg criterion that the chain is typically well described by the previous mean-field approximation. The model examples computed in this paper use parameters that are all within expected physiological bounds.

Taken in combination with the previous analytical treatments, these Monte Carlo calculations provide a nearly complete description of the mechanical properties of the HCWLC model for α-helical polypeptides. It remains only to develop a full, three-dimensional description of the polymer that incorporates the torsional degrees of freedom into the problem as well as to address the role of chemical heterogeneity in order to develop a complete and rather general equilibrium description of these biopolymers.

ACKNOWLEDGMENTS

We thank Professor J. Machta for stimulating conversations regarding this work. B.C. also thanks Professor N. Prokofev and B. Svitsunov for helpful discussions and for the use of computational resources. B.C. acknowledges the hospitality of the Indian Institute of Science, Bangalore, and UCLA Department of Chemistry. A.J.L. acknowledges the National Central University, Taiwan, where parts of this work were done.

[1] O. Kratky and G. Porod, Rev. Trav. Chim. **68**, 1106 (1949).
[2] M. E. Fisher, Am. J. Phys. **32**, 343 (1963).
[3] S. Smith, L. Finzi, and C. Bustamante, Science **258**, 122 (1992).
[4] T. T. Perkins, S. R. Quake, D. E. Smith, and S. Chu, Science **264**, 822 (1994).
[5] T. T. Perkins, D. E. Smith, R. G. Larson, and S. Chu, Science **268**, 83 (1995).
[6] P. Cluzel, A. Lebrun, C. Heller, R. Lavery, J.-L. Viovy, D. Chatenay, and F. Caron, Science **271**, 792 (1996).
[7] T. Strick, J. Allemand, D. Bensimon, A. Bensimon, and V. Croquette, Science **271**, 1835 (1996).
[8] T. T. Perkins, D. E. Smith, and S. Chu, Science **276**, 2016 (1997).
[9] C. Bustamante, Z. Bryant, and S. B. Smith, Nature (London) **421**, 423 (2003).
[10] T. R. Strick, M-N. Dessinges, G. Charvin, N. H. Dekker, J.-F. Allemand, D. Bensimon, and V. Croquette, Rep. Prog. Phys. **66**, 1 (2003).
[11] H. Benoit and P. M. Doty, J. Chem. Phys. **57**, 958 (1953).
[12] J. F. Marko and E. Siggia, Macromolecules **28**, 8759 (1995).
[13] M. Rief, H. Clausen-Schaumman, and H. E. Gaub, Nat. Struct. Biol. **6**, 346 (1990).
[14] P. Cizeau and J.-L. Viovy, Biopolymers **42**, 383 (1997).
[15] T. Cloutier and J. Widom, Mol. Cell **14**, 355 (2004).
[16] P. A. Wiggins, R. Phillips, and P. C. Nelson, Phys. Rev. E **71**, 021909 (2005).
[17] J. S. Mills and J. D. Johnson, J. Biol. Chem. **260**, 15100 (1985).
[18] M. Zhang and T. Yuan, Biochem. Cell Biol. **76**, 313 (1998).
[19] W. Wriggers, E. Mehler, F. Pitici, H. Weinstein, and K. Schulten, Biophys. J. **74**, 1622 (1998).
[20] B. F. Volkman, D. Lipson, D. E. Wemmer, and D. Kern, Science **291**, 2429 (2001).
[21] A. J. Levine, e-print cond-mat/0401624.
[22] B. Chakrabarti and A. J. Levine, Phys. Rev. E **71**, 031905 (2004).
[23] C. Storm and P. C. Nelson, Phys. Rev. E **67**, 051906 (2003).
[24] P. M. Chaikin and T. C. Lubensky, *Principles of Condensed Matter Physics* (Cambridge University Press, Cambridge, U.K., 1998).
[25] F. C. MacKintosh, J. Käs, and P. A. Janmey, Phys. Rev. Lett. **75**, 4425 (1995).
[26] A. Lamura, T. W. Burkhardt, and G. Gompper, Phys. Rev. E **64**, 061801 (2001).
[27] D. Poland and H. A. Scheraga, *Theory of Helix-Coil Transitions in Biopolymers: Statistical Mechanical Theory of Order-Disorder Transitions in Biological Molecules* (Academic Press, New York, 1970).
[28] T. M. Birshtein and O. Ptitsyn, *Conformations of Macromolecules* (Wiley, New York, 1966).
[29] V. A. Bloomfield, Am. J. Phys. **67**, 1212 (1999).
[30] M. N. Tamashiro and P. Pincus, Phys. Rev. E **63**, 021909 (2001).
[31] R. D. Kamien, T. C. Lubensky, P. Nelson, and C. S. O'Hern, Europhys. Lett. **38**, 237 (1997).
[32] C. S. O'Hern, R. D. Kamien, T. C. Lubensky, and P. Nelson, Eur. Phys. J. B **1**, 95 (1998).
[33] B. Chakrabarti and A. J. Levine (unpublished).
[34] P. Debye, Phys. Z. **28**, 135 (1927).
[35] T. Arakawa and S. N. Timasheff, Biochemistry **23**, 5924 (1984).
[36] A.-S. Yang and B. Honig, J. Mol. Biol. **252**, 351 (1995).
[37] A. Chakrabartty, T. Kortemme, and R. L. Baldwin, Protein Sci. **3**, 843 (1994).
[38] D. A. Smith, D. J. Brockwell, R. C. Zinober, A. W. Blake, G. S. Beddard, P. D. Olmsted, and S. E. Radford, Philos. Trans. R. Soc. London, Ser. A **361**, 713 (2003).
[39] E. Evans and K. Ritchie, Biophys. J. **72**, 1541 (1999).